

Oscillation properties of relativistic tori in the vicinity of a distorted deformed compact object

Shokoufe Faraji* and Audrey Trova†

University of Bremen, Center of Applied Space Technology and Microgravity (ZARM), 28359 Germany

This paper studies the oscillation properties of relativistic, non-self-gravitating tori in the background of a distorted deformed compact object. This work concentrates on the static and axially symmetric metric containing two quadrupole parameters; relating to the central object and the external fields. This metric may associate the observable effects to these parameters as dynamical degrees of freedom. The astrophysical motivation for choosing such a field is the possibility of constituting a reasonable model for an actual scenario occurring in the vicinity of compact objects. This paper aims to investigate the radial epicyclic frequency in a perfect fluid disk and not a test particle scenario via a local analysis. To achieve this goal, we employ the vertically integrated technique to able to treat the equation analytically. The tori are also modelled with Keplerian and non-Keplerian distributions of specific angular momentum, and we discuss the dependence of oscillation properties on the variable of the model related to angular momentum distribution and quadrupoles. In the present contribution, we further explore these properties with the possibility of relating oscillatory frequencies to some high-frequency quasi-periodic oscillations models and observed data.

I. INTRODUCTION

Most of the black hole binaries accompanied by rapid variations in the x-ray emission on different time scales [1–4]. The important features of the X-ray emission from these systems is quasi-periodic oscillations (QPOs). The QPOs have been detected for several black hole binaries and they are classified as low frequency QPOs (≤ 30 Hz) and high frequency QPOs (≥ 60 Hz).

There is a good agreement that strong correlations exist between the QPOs frequency and the accretion disc parameters like inner disc radius; however, the physics of their origin is not yet clear. Therefore, QPOs can provide a possibility to probe the strong gravity near compact objects. They also may be used to calculate the spin and mass of the compact object. Several models try to explain QPOs based on the geometrically thin and optically thick accretion disc, which are truncated at a radius greater than the innermost stable circular orbit. For example, the Relativistic Precession model (RPM) assumes QPOs are produced by a local motion of accreted inhomogeneities and tries to relate the QPO frequencies to the Keplerian and periastron precession frequency [5, 6]. In this respect, the properties of the orbital motion frequencies have been extensively studied [7–20] among many others.

During these years, this model modified in different ways. For example, a different class presented the collective motion of accreted matter considering normal modes of thin accretion disk oscillations, also slender and non-slender tori oscillations e.g. [21–30]. In particular, oscillations of geometrically thick discs are notable since this disk can radiate significantly and they reveal a long-term oscillatory behaviour with the duration of tens of

orbital periods. The oscillation modes of geometrically thick discs are studied through the vertically averaging technique and local perturbative analyses in [31–33]. In these works, the expression of the radial epicyclic frequency is derived for a fluid disk in these works. In fact, for interpreting the observed QPOs frequencies, maybe one important consideration is to pay attention to using the expression of the radial epicyclic frequency for a test particle. Therefore, one further step can be the investigation of the radial epicyclic frequency in a perfect fluid disk. This paper aims to extend this approach with different angular momentum distributions to the background of a distorted deformed compact object due to quadrupoles. We studied the QPOs with the test particle approach in this background in [34]. Indeed, in the astrophysics area, people attempt to determine the observable predictions of strong-field images of accretion flows in many ways. In this respect, this approach may provide an opportunity to take quadrupole moments as the additional physical degrees of freedom to the central compact object and its surroundings. Moreover, there is no doubt about the fundamental importance of gravitational waves in physics, where the experimental evidence finally supported the purely theoretical research in this area [35]. In fact, in the case of extreme mass ratio inspiral (EMRI), one can extract the multipole moments from the gravitational wave signal, and any non-Kerr multipole moments should be encoded in the waves [36]. A study of gravitational waves generated in an EMRI is in progress. This space-time is briefly described in Section III. In addition, we examine the results of this study by using the data of three high-frequency QPOs observed in the microquasars GRS 1915+105, XTE 1550-564 and GRO 1655-40.

The plan of the paper is as follows. In Section II we briefly explain the relativistic tori model and the local perturbation approach. In Section III the desired background is explained. Results and discussion is presented in Section IV. Finally, the conclusion is summarized in

* shokoufe.faraji@zarm.uni-bremen.de

† audrey.trova@zarm.uni-bremen.de

Section V. In this work, we use the metric signature as $(-, +, +, +)$ and geometrized unit system $G = 1 = c$ (However, for an astrophysical application, we will use SI units). Latin indices run from 1 to 3, while Greek ones take values from 0 to 3.

II. PERTURBATION OF RELATIVISTIC TORI

The relativistic tori in a stationary and axisymmetric space-time, is the configuration of the perfect fluid described by polytropic equation of state of this type $p = k\rho^\gamma$, with the polytropic constant k and the adiabatic index $\gamma = \frac{d \ln p}{d \ln \rho}$. This equation implies the conservation of entropy for a perfect fluid. The fluid is determined by its rotation in the azimuthal direction with the four-velocity, specific angular momentum and the angular velocity

$$u^\mu = (u^t, 0, 0, u^\phi), \quad (1)$$

$$l = -\frac{u_\phi}{u_t}, \quad (2)$$

$$\Omega = \frac{u^\phi}{u^t}. \quad (3)$$

The shape of the tori with rest-mass density ρ is determined by equi-pressure surfaces profile which specify by the basic conservation equations

$$\nabla_\beta(\rho u^\beta) = 0, \quad (4)$$

$$\nabla_\beta T^{\beta\alpha} = 0. \quad (5)$$

where ∇ is the covariant derivative, and $T^{\beta\alpha}$ is the stress-energy tensor

$$T^{\beta\alpha} = \omega u^\beta u^\alpha + p g^{\beta\alpha}, \quad (6)$$

where ω is the enthalpy and p is the pressure. From these relation the Bernoulli-type equations follows for pressure distribution [37]

$$\frac{1}{\omega} \nabla_i p = -\nabla_i \ln u_t + \frac{\Omega \nabla_i l}{1 - \Omega l}. \quad (7)$$

In order to integrate and solve this equation analytically, we need to consider $\Omega = \Omega(l)$ and determine distribution of angular momentum. Of course, the simplest choice for l to have a finite disc size is being a constant, say l_{cons} . chosen between the specific angular momentum at the marginally stable orbit l_{ms} and the specific angular momentum at the marginally bound orbit l_{mb} . However, in what follows we also consider non-constant angular momentum. In addition, there are two important locations in this model; namely the cusp, r_{cusp} and the center r_c . They are defined as the places when the Keplerian specific angular momentum is equal to l_{cons} . The center is defined as where we have the maximum

density in the torus. The inner and outer edges of the tori can be specify by asking they lie on the same equipotential surface. In this work, we also worked with a non-constant angular momentum distribution in which it has two important properties features of the angular momentum distribution in accretion disks. This distribution on the equatorial plane and far from the object is slightly sub-Keplerian, but closer it becomes slightly super-Keplerian and in the plunging region, it becomes again sub-Keplerian and almost constant [38]

$$\ell(r, \theta) = \begin{cases} \ell_0 \left(\frac{\ell_{\text{K}(r)}}{\ell_0} \right)^\gamma \sin^{2\delta}, & r \geq r_{\text{ms}}, \\ \ell_0 (\zeta)^{-\gamma} \sin^{2\delta}, & r < r_{\text{ms}}, \end{cases} \quad (8)$$

where $\ell_0 = \zeta \ell_{\text{K}}(r_{\text{ms}})$, and ℓ_{K} is the Keplerian angular momentum in the equatorial plane, and

$$0 \leq \gamma \leq 1, \quad -1 \leq \delta \leq 1, \quad -1 \leq \zeta \leq \frac{\ell_{\text{K}}(x_{\text{mb}})}{\ell_{\text{K}}(x_{\text{ms}})}. \quad (9)$$

where $\ell_{\text{ms}}(r)$ is calculated on the equatorial plane via considering Ω_{ms} . In the following subsection, we introduce the local perturbations in this background following the procedure in [32, 33].

A. Local perturbation

In this method, to reduce one spatial dimension for simplicity to solve analytically, the vertically integrated and vertically averaged technique along the direction perpendicular to the equatorial plane is assumed for quantities. Beside, the local approach leads to derive the local dispersion relation for the oscillations in relativistic non-Keplerian discs in a given background.

In the following we discuss briefly the local perturbation approach for the circular orbiting test particle and a perfect fluid. However, instead of power-law angular momentum distribution used in [32, 33], here we used the one that mentioned earlier via the equation (8).

In this approach, we are interested in the vicinity of the equatorial plane $|y - 0| \ll 1$, which is different from consider just the equatorial plane of course since here use the vertically integrated quantities corresponding to collapsing the vertical structure of the tori on the equatorial plane and not just consider the equatorial slice of the tori and calculate the quantities in the equatorial plane. This approach is very similar to the technique used for the Thin accretion disk [39, 40].

Following [32] we introduce the vertically integrated pressure P , rest-mass density Σ , velocity components $U(r)$ and $W(r)$ in terms of the local thickness $H = H(r)$ of tori, respectively as

$$P(r) := \int_{-H}^H p dz, \quad (10)$$

$$\Sigma(r) := \int_{-H}^H \omega dz, \quad (11)$$

$$U(r) := \frac{1}{2H} \int_{-H}^H v^r dz, \quad (12)$$

$$W(r) := \frac{1}{2H} \int_{-H}^H v^\phi dz, \quad (13)$$

where v^i are the three-velocity of the fluid. We also need to modify the equation of state in a consistent way. To do so we define the adiabatic index $\Gamma = \frac{d \ln P}{d \ln \Sigma}$ so that

$$P = \mathcal{K} \Sigma^\Gamma, \quad (14)$$

where \mathcal{K} is the corresponding polytropic constant. However, equation (14) does not represent a vertically integrated polytropic equation of state if $\Gamma \neq 1$. In addition, to get rid of the height dependence of $\Gamma = \Gamma(r, z)$ for simplicity one can assume p and ρ have a weak dependence on height, so that they can be stated in terms of their values at the equatorial plane. Therefore, we can use this modified expression for the equation of state

$$P = k \Sigma^\gamma. \quad (15)$$

With these quantities the dynamics of the torus is fully determined [32, 41] once we choose the parameters of the model. Next, we introduce harmonic Eulerian perturbations

$$\begin{pmatrix} \delta U \\ \delta W \\ \delta Q \end{pmatrix} \sim e^{-i\sigma t + ikr} \quad (16)$$

where for the the fluid pressure we consider

$$\delta Q = \frac{\delta P}{\Sigma}. \quad (17)$$

In fact, the harmonic spatial dependence in this relations as the signature of the local perturbation is valid for when the wavelength of the perturbations is smaller than the radial variations in the equilibrium configuration, the Wenzel–Kramers–Brillouin (WKB) approximation. By applying the above perturbations in the equilibrium tori model and considering only up to the first-order terms and neglecting the time derivatives, we derive the perturbation equations [32]. This linear system of differential equations has a non-trivial solution by searching for the zeros of determinants of coefficients matrix, which simply leads to the dispersion relation

$$\sigma^2 = \kappa^2 + f(r)k^2c_s^2, \quad (18)$$

where k_r is the radial epicyclic frequency, and c_s is the local sound velocity. The function $f(r)$ in this relation changes for different backgrounds. In Newtonian set-up $f(r) = 1$ and has different expression in Schwarzschild space-time [32, equation 42], or in the Kerr space-time [33, equation 17]. Moreover, it is assumed that the perturbation wavelength is much smaller than the radius of the disk, and the imaginary part of the epicyclic frequency is also neglected [32].

In fact, the first term in the dispersion relation is the radial oscillation of a fluid element when due to a restoring centrifugal force, it is infinitesimally displaced from its equilibrium with no change in the angular momentum. This produces inertial oscillations with the frequency κ . However, there exist also a vertical epicyclic frequency with an amplitude much smaller than the radial one [42], therefore we neglected here. The second term, the frequency kc_s is due to pressure gradients in compressible fluids that leads to the acoustic oscillations [43].

To study the radial epicyclic oscillation in this approach, one can consider different angular momentum distributions. However, for the Keplerian angular momentum distribution where $\Omega \propto r^{-\frac{3}{2}}$ the radial epicyclic frequency is equal to the orbital frequency $\kappa_r^2 = \Omega^2$. Besides, the radial epicyclic frequency vanishes for the constant specific angular momentum dictating by the corresponding equations [32, 33]. Thus, for this investigation we used non-constant angular momentum distribution presented in [38]. In the next section, the background space-time that we are interested to consider in this work is briefly explained.

III. SPACE-TIME

In many years, the Weyl's family of solutions [44] to the static vacuum Einstein equations, have been used to modeling the exterior gravitational field of compact axially symmetric bodies. In this regard, the simplest and applicable generalization of the Schwarzschild family is the q-metric. It describes static, axially symmetric, and asymptotically flat solutions with quadrupole moment describing the deviation from the spherical body. The metric represents the exterior gravitational field of an isolated compact object [45–48]. This metric has been further generalized by relaxing the assumption of isolated compact object via considering the exterior distribution of mass in its vicinity. It is similar to considering additional external gravitational field, like adding a magnetic surrounding [49]. This generalization is also characterising by quadrupole [50]. In fact, the presence of a quadrupole, can change the geometric properties of space-time drastically. The metric in the prolate spheroidal coordinates is presented as follows [50]

$$\begin{aligned}
ds^2 = & - \left(\frac{x-1}{x+1} \right)^{(1+\alpha)} e^{2\hat{\psi}} dt^2 + M^2 (x^2 - 1) e^{-2\hat{\psi}} \\
& \left(\frac{x+1}{x-1} \right)^{(1+\alpha)} \left[\left(\frac{x^2-1}{x^2-y^2} \right)^{\alpha(2+\alpha)} e^{2\hat{\gamma}} \right. \\
& \left. \left(\frac{dx^2}{x^2-1} + \frac{dy^2}{1-y^2} \right) + (1-y^2)d\phi^2 \right], \quad (19)
\end{aligned}$$

where $t \in (-\infty, +\infty)$, $x \in (1, +\infty)$, $y \in [-1, 1]$, and $\phi \in [0, 2\pi)$. Also $\alpha \in (-1, \infty)$ is the quadrupole associated with the central compact object. Nevertheless, we consider relatively small quadrupole moment; therefore, a physically interior solution can be fit to this external solution [47]. quadrupole α determines the deviation from spherical shape and how the mass distribution is stretched-out along some axis. If $\alpha > 0$ we have an oblate object and for $\alpha < 0$ we have a prolate shape. If $\alpha = 0$, $\hat{\psi} = 0$, $\hat{\gamma} = 0$ the Schwarzschild metric is recovered. Up to the quadrupole the external field terms read as follows

$$\begin{aligned}
\hat{\psi} &= -\frac{\beta}{2} [-3x^2y^2 + x^2 + y^2 - 1], \\
\hat{\gamma} &= -2x\beta(1+\alpha)(1-y^2) \\
&+ \frac{\beta^2}{4}(x^2-1)(1-y^2)(-9x^2y^2 + x^2 + y^2 - 1), \quad (20)
\end{aligned}$$

where β is the quadrupole associated with the external fields. To have some intuitive picture about the role of β we can consider Newtonian gravity (we show quadrupole

in Newtonian picture by β_N). In Newtonian theory it is rather familiar piece of knowledge that the multipole expansion dominated by a quadrupole moment β_N can be modelled by two equal point-like masses m located on some axis, say z , at some distance from the center, also an infinitesimally thin ring of the mass M and radius R located at the plane perpendicular to this axis. If the contribution of the point-like masses to the gravitational field is greater than the ring, then $\beta_N < 0$, and if for ring is greater we have $\beta_N > 0$. If $\beta_N < 0$, then there exist a net force directed toward the z -axis. This force creates a potential barrier. If $\beta_N > 0$, there is a net force directed to the ring, outward from the central object. This force balances the gravitational of the central source and the external fields.

The relation between this coordinates system and the Schwarzschild like coordinates is given by

$$x = \frac{r}{M} - 1, \quad y = \cos \theta. \quad (21)$$

In the following we present the relativistic tori in this background and analysis the epicyclic frequencies as mentioned earlier.

IV. RESULTS AND DISCUSSION

Before start studying the epicyclic frequency we investigate the model in this background briefly.

A. Relativistic tori

The equation (7) for radial component in this background obtained as

$$\frac{1}{\omega} \partial_r p = \frac{r \left(\frac{r}{r-2} \right)^\alpha (\alpha - (r-2)(1 + \beta(r-1)r)) \Omega^2 + e^{-\beta(r-2)r+2\hat{\psi}} (r-2)^{1+\alpha} r^{-2-\alpha} (1 + \alpha + (r-2)r\partial_r \hat{\psi})}{(r-2) \left(-e^{-\beta(r-2)r+2\hat{\psi}} \left(\frac{r-2}{r} \right)^{1+\alpha} + r^2 \left(\frac{r}{r-2} \right)^\alpha \Omega^2 \right)}. \quad (22)$$

As it pointed out, to be able to integrate and solve this equation one needs to specify the angular momentum distribution. In this work, first we consider constant distribution to see the effects of quadrupoles in the metric, and then used the distribution in the equation (8). Figure 1 shows the disk configuration for $\ell_{\text{cons.}} = (\ell_{\text{ms}} + \ell_{\text{mb}})/2$, where ℓ_{mb} and ℓ_{ms} are calculated for chosen values of quadrupoles written on the plots. In this Figure we can see the influence of quadrupoles on the shape and size of the tori. We see that, in general, for negative α which is correspond to prolate object we have larger size disk rather than Schwarzschild and positive ones. For $\alpha > 0$ the disk is smaller and is formed far from the central object comparing to negative α . On the other hand, having positive quadrupole in the external field $\beta > 0$ causes to

have a bigger disk structure and more extended radially. However, it is worth mentioning that the overall shape of disk is more influenced by α which is the quadrupole links to the central object. In Figure 2 we see the disk configuration in the present of different angular momentum. In this Figure, we used the same values for quadrupoles as in Figure 1 to see the effect of angular momentum distribution clearly. We see that choosing the angular momentum profile has a strong effect on the shape and size of the disk. The parameters of this distribution have a strong correlation with each other. However, as we chose higher values for this pairs (γ, δ) the disc configuration become smaller.

In the following we study the epicyclic radial frequency. As discussed earlier for a constant angular momentum

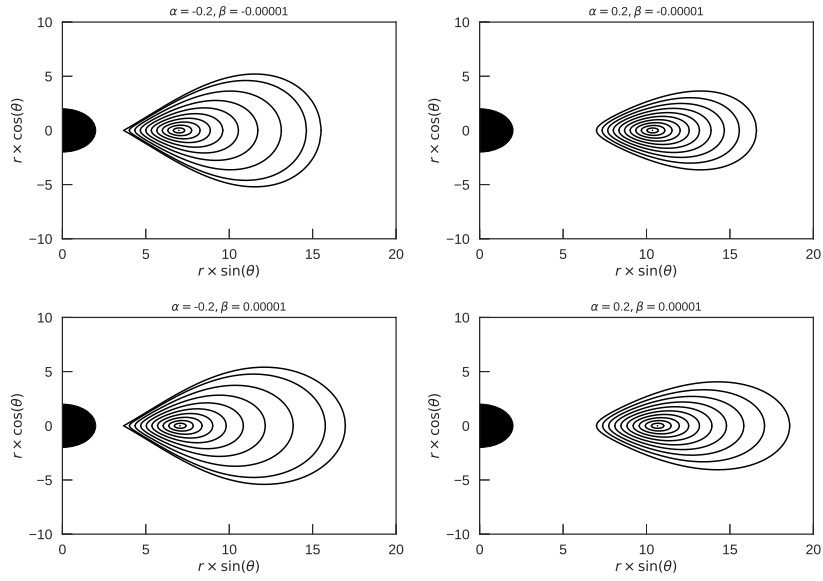


FIG. 1. Equipotential surfaces for tori with a constant angular momentum distribution $\ell_{\text{cons.}} = (\ell_{\text{ms}} + \ell_{\text{mb}})/2$ for different values of α and β .

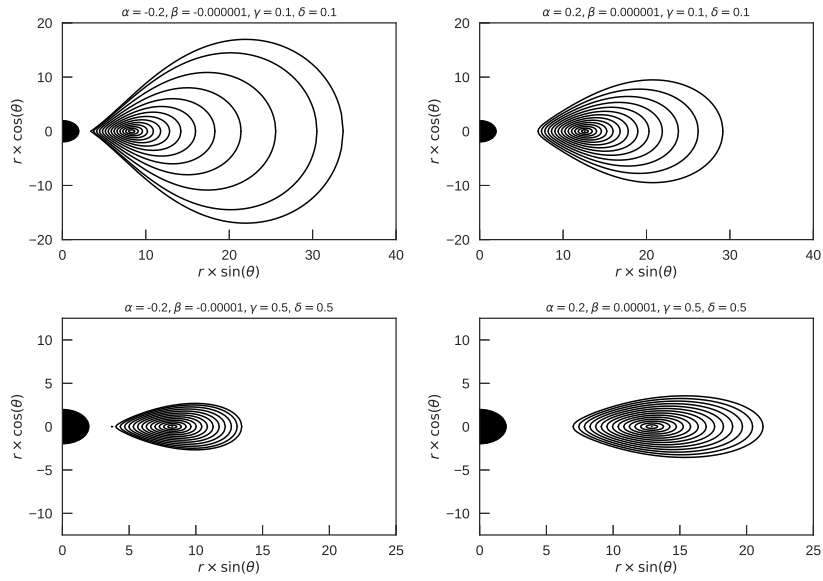


FIG. 2. Equipotential surfaces for tori with the non-constant angular momentum distribution for various values of combination of α and β .

profile $\kappa = 0$. Then we adopt the equation (8) for angular momentum distribution in the rest of this work.

B. Radial epicyclic frequency

To investigate the radial epicyclic frequency in a perfect fluid disk, considering the method described in Subsection II A, finally the relation of κ for the tori, in this space-time is obtained as follows

$$\kappa^2 = \frac{2e^{\beta(x^2-1)+2\nu-2\lambda} \left(\frac{x+1}{x-1}\right)^\alpha \Omega V (-2\Omega V + (x^2-1)\partial_x \Omega)}{F}, \quad (23)$$

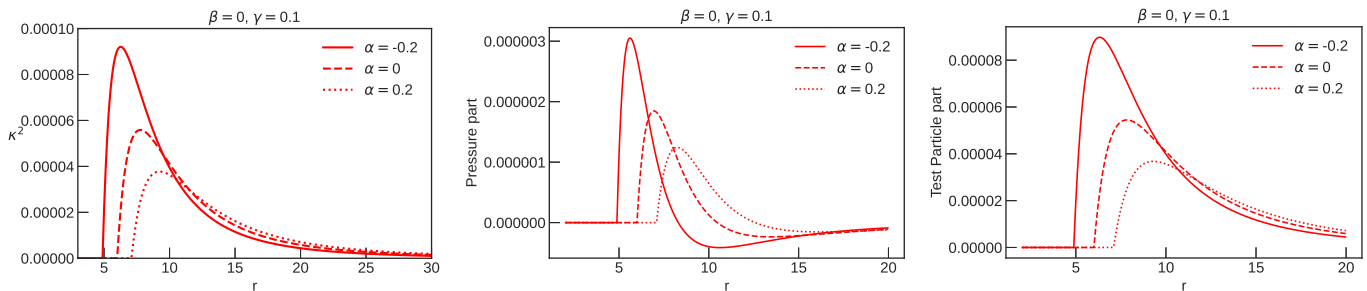


FIG. 3. The plots present the radial epicyclic frequency squared with respect to r with $\gamma = 0.1$ in the angular momentum distribution (8) for different values of α . The right one shows κ_t^2 for a test particle (equation 25). The middle one presents κ_p^2 corresponds to the pressure part, and the left one the κ^2 for the fluid.

where

$$V = \underbrace{1 + \alpha + (\beta - 1)x - \beta x^3}_{V_1} + \underbrace{(x^2 - 1)\partial_x \nu}_{V_2} \quad (24)$$

$$F = (x^2 - 1) \left(-e^{2\nu} + e^{\beta(x^2-1)}(x+1)^2 \left(\frac{x+1}{x-1} \right)^\alpha \Omega^2 \right),$$

$$\nu = \left(\frac{1 + \alpha}{2} \right) \ln \frac{x-1}{x+1} + \hat{\psi}$$

$$\lambda = \left(\frac{1 + \alpha}{2} \right) \ln \frac{x+1}{x-1} + \left(\frac{\alpha(2 + \alpha)}{2} \right) \ln \frac{x^2 - 1}{x^2} - \hat{\psi} + \hat{\gamma}.$$

If we consider the κ squared, this radial epicyclic frequency can be written in terms of superposition of two parts. First related to the test particle and the second related to when we consider the pressure in the disk

$$\kappa^2 = \kappa_t^2 + \kappa_p^2, \quad (25)$$

where

$$\kappa_t^2 = \frac{2e^{q(x^2-1)-2\lambda} \left(\frac{x+1}{x-1} \right)^p \Omega V_1 (2\Omega V - (x^2 - 1)\partial_x \Omega)}{(x-1)^2}, \quad (26)$$

$$\kappa_p^2 = \frac{2e^{2q(x^2-1)-2\lambda} \left(\frac{x+1}{x-1} \right)^p \Omega}{F} \left[(x+1)^2 \left(\frac{x+1}{x-1} \right)^p V_1 \Omega^2 + e^{-q(x^2-1)+2\nu} V_2 \right] (-2\Omega V + (x^2 - 1)\partial_x \Omega). \quad (27)$$

In Figure 3 we see κ^2 plotted for the vanishing external field $\beta = 0$, and for different negative, positive values of α , and the Schwarzschild case $\alpha = 0$. The parameter γ is the angular momentum distribution variable that we discussed so far. First of all because of vertically integration that we are interested in a neighborhood of equatorial plane δ plays no role; however, we have its contribution in the disk configuration. Figure 4 presents κ^2 for two different values of γ ; in addition, we can compare the κ^2 for a fluid constructed by a non-constant angular momentum depicted in red (equation (8)) with κ^2 for a test

particle with the Keplerian angular momentum in blue. In general, larger parameter γ has more influence as we go far from the central object which is compatible with its definition (8). Besides, considering Figures 3 and 4 together reveal the effect of different angular momentum on the radial epicyclic frequency of a test particle, which is consistent with what we saw from Figures 2 and 1.

The important key here is in general theory of relativity κ does not increase as we go closer and closer to the central object, but instead have a maximum at a few gravitational radii before the innermost stable circular orbit (ISCO) where consider as a very good estimation of the inner edge of the disc, and it is zero at the ISCO. Therefore, oscillations in this part of the disk may trap and lead to the periodic flux variations which we can observe [51]. However, this is not the case in the Newtonian gravity. For instance, Figure 5 for different range of quadrupole parameters shows the maximum of κ appears before the place of ISCO in each case. It is worth mentioning that the place of ISCO is dependent on quadrupole moments and this is closer to the central source for negative ones [52]. In this Figure, the red line depicted the place of ISCO and the black line the place of κ maxima for a test particle.

One can see the influence of different sign of parameter β , as well as α on the radial epicyclic frequency κ for tori in Figure 6. We see that for both $\alpha < 0$ and β the maximum is higher than for their zero and positive values, also it is more closer to the central object. Furthermore, there is an interesting fact about positive quadrupole β . When β is positive the radial epicyclic frequency terminates much faster regardless of sign of α . As we discuss it in Newtonian picture, this is the manifestation of the external field when the ring like part is greater.

C. QPO models and observation

In this section, we study the epicyclic modes of relativistic tori oscillations in the context of the observed QPO frequencies. One can assume that the two oscillatory modes identified with the observed 3 : 2 QPOs are excited at the same radius and physical conditions,

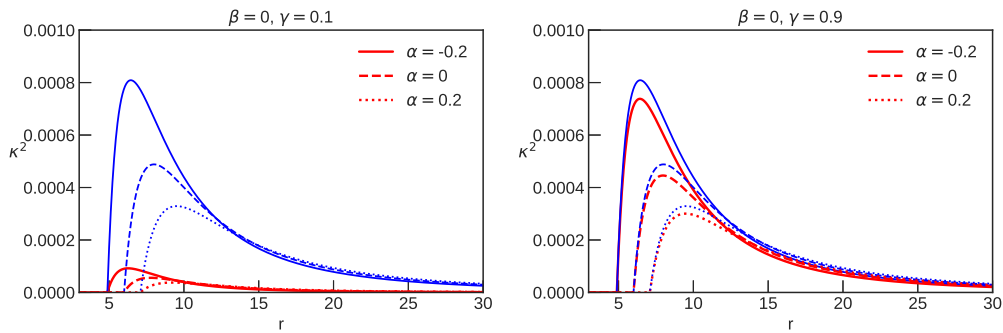


FIG. 4. The plots of κ^2 for the tori are presented in red to compare with the blue one κ^2 for the test particle and with Keplerian angular momentum. In addition, two different parameters of γ related to angular momentum are considered. For higher γ we have radial epicyclic frequency approaching the Keplerian one which is compatible with its definition.

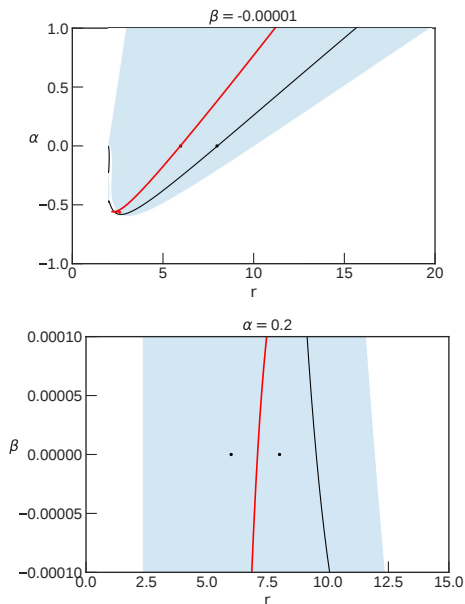


FIG. 5. The red line presents the place of ISCO with respect to α and β . The black line depicts the value of the maxima of κ . The blue region shows where κ can exhibit maxima. The two dots give, from left to right, ISCO and the maximum of κ for the Schwarzschild case.

which is also valid for a broader class of models [30]. In this sense, our study is relevant to the consideration of the epicyclic oscillation modes in this context. In principle, different classes of QPO models, assume a relation between the epicyclic frequencies of a particle motion and QPO frequencies [25, 53–55]. To summarise them, the eigenfrequencies of two modes in resonance should be equal to the radial epicyclic frequency and the vertical epicyclic or to the Keplerian frequency [53, 56, 57]. The parametric resonance models identify the two observed frequencies of (ν_U, ν_L) with the eigenfrequencies of the resonance. However, none of these models is well-matched, especially with the full QPOs amplitudes and the visibility on the source spectral data, in the LMXBs,

and this area of research is a non complete task.

In the following, we consider kinematic models RP and TD, and the resonant models WD and Kp. The Relativistic Precession Model (RP) is one of the first attempts proposed in [6, 58]. In RP model $\nu_U = \Omega$ and $\nu_p := \nu_L = \Omega - \nu_x$. Their correlations are obtained by varying the radius of the associated circular orbit. It is usually assumed that the variable component of the observed X-ray arises from the motion of “hot-spots” or biting inside the accretion disk on a slightly eccentric orbit. The Epicyclic resonance Model (kp) [53] defines the upper frequency as $\nu_U = \Omega$ and the lower frequency as $\nu_L = \omega_x$. The Tidal Disruption Model (TD), a kinematic model [59, 60] follows very similar approach as the RPm. In this model, the QPOs are assumed as a result of tidal disruption of large accreting inhomogeneities. In TDM the frequencies are identified with $\nu_U = \Omega + \omega_x$ and $\nu_L = \Omega$. The Warped disc Model (WDM) is related to non-axisymmetric modes in a warped accretion disc [61]. In WDM the frequencies are defined as $\nu_U = 2\Omega - \omega_x$ and $\nu_L = 2\Omega - 2\omega_x$. In more realistic versions of this model, the higher harmonic oscillations are also considered up to the third order, then frequencies like $3\Omega - \omega_x$ possible to consider. The weakness of this model is it considers a somehow exotic disc geometry that causes a doubling of the observed lower QPO frequency.

In the Figure 7, one of the primary focuses is on the influence of the variation of parameters in the angular momentum distribution on the radial epicyclic frequency of the fluid κ and Ω . We can note that when increasing γ , κ for the fluid approach goes closer to the test-particle case. This feature is expected since when γ is increasing it approaches the Keplerian Angular momentum. About the Ω the behaviour is similar. We can add that at some radius (bigger radius when increasing β) the black lines are decreasing faster than the red ones and in consequence crossing each other.

The second point here is about the ratio between these two frequencies and particularly about the 3 : 2 ratio between them. For each model, the chosen upper frequency ν_U is a function of the inverse of the mass M of the cen-

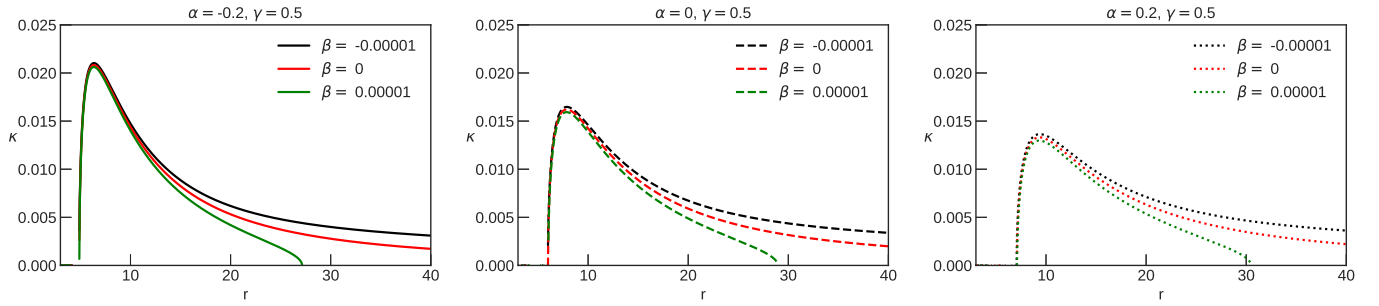


FIG. 6. The plots of κ for tori with respect to r for various combination of β , α and γ .

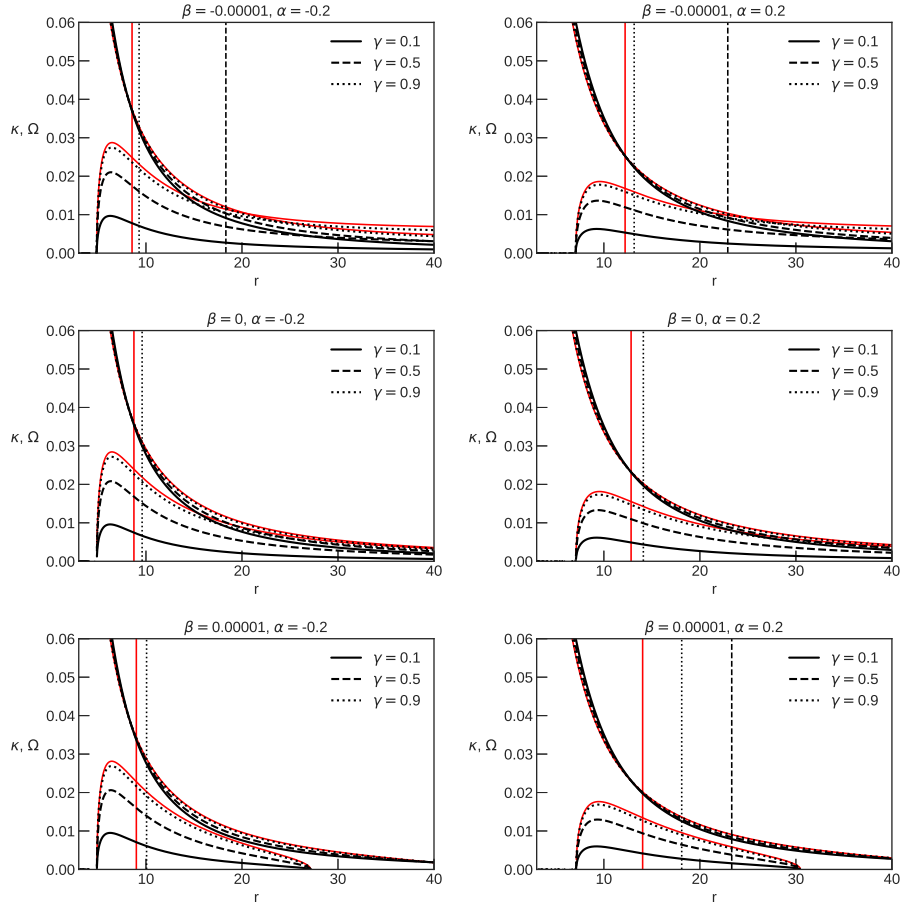


FIG. 7. κ and Ω (monotonic curves) with respect to r for tori and different values of α , β and γ . The red lines are respectively κ and Ω for the test particle case. The vertical line corresponds to the radius of the 3 : 2 ratio between Ω : κ for KP model.

tral object scaled by a constant related to $\Omega(r_*)$ where r_* is the radius of the ratio between the upper and lower frequency. In the particular case of the *KP* model, $\nu_U \sim \Omega$ and $\nu_L \sim \kappa$. The vertical line in the figure 7 are corresponding to the radius, r_* , of the 3 : 2 between Ω : κ . For certain values of γ , depending on the metric parameters, the corresponding vertical lines do not appear on the plots. There are two reasons: (i) the 3 : 2 ratio is not possible which can happen for positive values of β since for a larger radius κ can become negative, and (ii)

the radius is far away than the horizontal range. We can see that the vertical line has the same behaviour as the frequencies, the ones related to the fluid are approaching closer and closer to the test particle ones. Besides, $\Omega(r_*)$ is bigger for the test particle than the tori. The related ν_U has the same steepness but shifted. This is shown in the Figure 8 for the *KP* model and in the Figures 9 and 10 for the *RP* and *TD* model, respectively. In this series of plots, we fit the upper frequency to the data of the three mentioned Microquasars I. All along these three

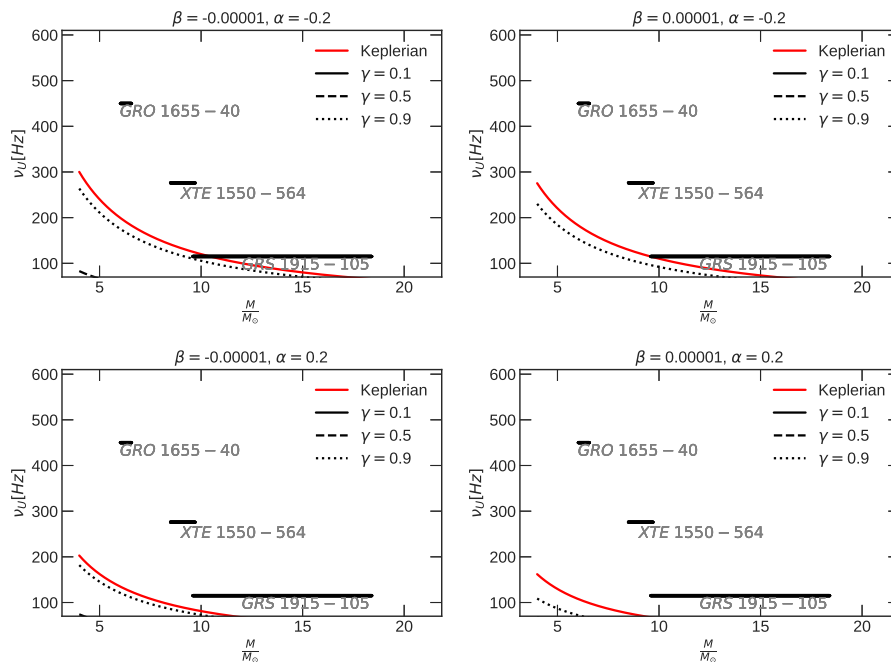


FIG. 8. The upper oscillation frequency ν_U at the resonance radius 3 : 2 is presented for various combinations of the studied parameters for the KP model. For the test-particle is depicted in red. The black lines present the fluid for various angular momentum. If the linestyle does not appear, it means that the chosen ratio 3 : 2 is not possible.

TABLE I. Observed HF QPO data for the three microquasars, independent of the HF QPO measurement, and based on the spectral continuum fitting.

Source	GRO 1655 – 40	XTE 1550 – 564	GRS 1915 + 105
ν_U	447 – 453	273 – 279	165 – 171
ν_L	295 – 305	179 – 189	108 – 118
$\frac{M}{M_\odot}$	6.03 – 6.57	8.5 – 9.7	9.6 – 18.4
a	0.65 – 0.75	0.29 – 0.52	0.98 – 1

figures, the legend follows the same pattern as Figure 7. We can see that in the Kp model, the combinations of the metric and angular momentum distribution parameters do fitting properly. The results are different when we move to the RP and TD models. For some sets of the various parameters, we have a much better crossing with the three data sets. The effect of the pressure, the angular momentum distribution and the metric parameters can not be decorrelated from each other. From the three Figures 8-10 a particular parameter α and γ coming from the metric and angular momentum distribution respectively, play a more major role in the fitting.

V. SUMMARY AND CONCLUSION

This paper studied the oscillation properties and examined different QPO models of relativistic, non-self-gravitating tori around a distorted deformed compact

object up to the quadrupole. This space-time is a generalization of the well-known q-metric which is static and axisymmetric and contains two distortion parameters β and deformation parameter α which is briefly explained in Section III. These two parameters alter the epicyclic frequencies' properties in this background.

The main goal of this paper was to study the radial epicyclic frequency in a perfect fluid disk via a local analysis analytically, and we derived the expression of the radial epicyclic frequency for the tori in the equation (23) since it was previously derived for a test particle [34]. To achieve this goal, we employ the vertically integrated technique for tori introduced in [32]. First, we built the tori with constant and non-constant angular momentum distribution [38] which is different from what is considered in [32, 33]. We discuss how the oscillation properties with parameters in the distributions of angular momentum.

Furthermore, we examined the possibility of relating oscillatory radial frequencies to the frequencies of the high-frequency quasi-periodic oscillations observed in three microquasars GRS 1915 + 105, XTE 1550 – 564, GRO 1655 – 40, and at their frequency ratio 3 : 2. In fact, this set-up may open up a variety of exciting applications in astrophysics due to presenting of quadrupole parameters in the model.

In fact, it is possible from observational data or other analytic set-ups to assign some restrictions on the parameters in this metric. Moreover, the next step of this work would be to explore more about the observational data by considering different inputs like rotation in this

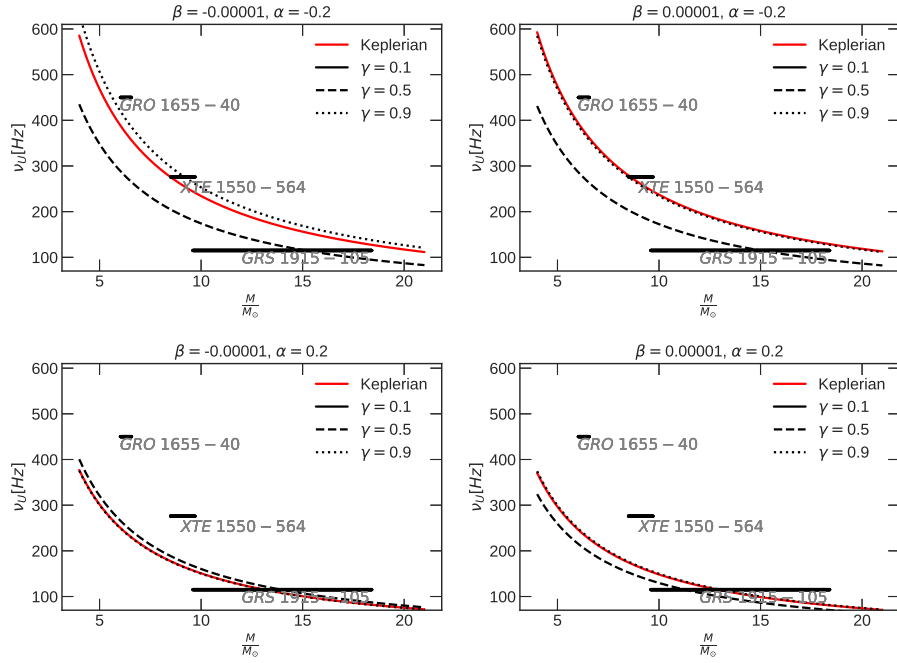


FIG. 9. The upper oscillation frequency ν_U at the resonance radius 3 : 2 is presented for various combinations of the studied parameters for the RP model. For the test-particle is depicted in red. The black lines present the fluid for various angular momentum. If the linestyle does not appear, it means that the chosen ratio 3 : 2 is not possible.

model that helps to model a more realistic complex system of astronomical objects. The perturbation study via a global approach and investigation of g-mode and p-mode oscillations in this background could be used to explain the harmonic relations in the observed HF QPOs. Also, adding the strong magnetic field, which influences the metric itself, is the subject of the following work.

ACKNOWLEDGMENTS

S.F. acknowledge the research training group GRK 1620 "Models of Gravity" and the excellence cluster

QuantumFrontiers funded by the Deutsche Forschungsgemeinschaft (DFG, German Research Foundation) under Germany's Excellence Strategy – EXC-2123 QuantumFrontiers – 390837967. A.T. is supported by the research training group GRK 1620 "Models of Gravity" funded by the DFG.

-
- [1] Dimitrios Psaltis, Tomaso Belloni, and Michiel van der Klis. Correlations in Quasi-periodic Oscillation and Noise Frequencies among Neutron Star and Black Hole X-Ray Binaries. *Astrophys. J.*, 520(1):262–270, July 1999.
 - [2] Adam Ingram, Chris Done, and P. Chris Fragile. Low-frequency quasi-periodic oscillations spectra and Lense-Thirring precession. *MNRAS*, 397(1):L101–L105, July 2009.
 - [3] Adam Ingram and Chris Done. A physical model for the continuum variability and quasi-periodic oscillation in accreting black holes. *MNRAS*, 415(3):2323–2335, August 2011.
 - [4] S. E. Motta. Quasi periodic oscillations in black hole binaries. *Astronomische Nachrichten*, 337(4-5):398, May 2016.
 - [5] Luigi Stella and Mario Vietri. Lense-Thirring Precession and Quasi-periodic Oscillations in Low-Mass X-Ray Binaries. *ApJ*, 492(1):L59–L62, January 1998.
 - [6] Luigi Stella and Mario Vietri. khz quasiperiodic oscillations in low-mass x-ray binaries as probes of general relativity in the strong-field regime. *Phys. Rev. Lett.*, 82:17–20, Jan 1999.
 - [7] A. N. Aliev and D. V. Galtsov. Radiation from relativistic particles in nongeodesic motion in a strong gravitational field. *General Relativity and Gravitation*, 13(10):899–912, October 1981.
 - [8] A. N. Aliev, D. V. Galtsov, and V. I. Petukhov. Negative Absorption Near a Magnetized Black-Hole - Black-Hole Masers. *Astrophys. Space Sci.*, 124(1):137–157, 1986.

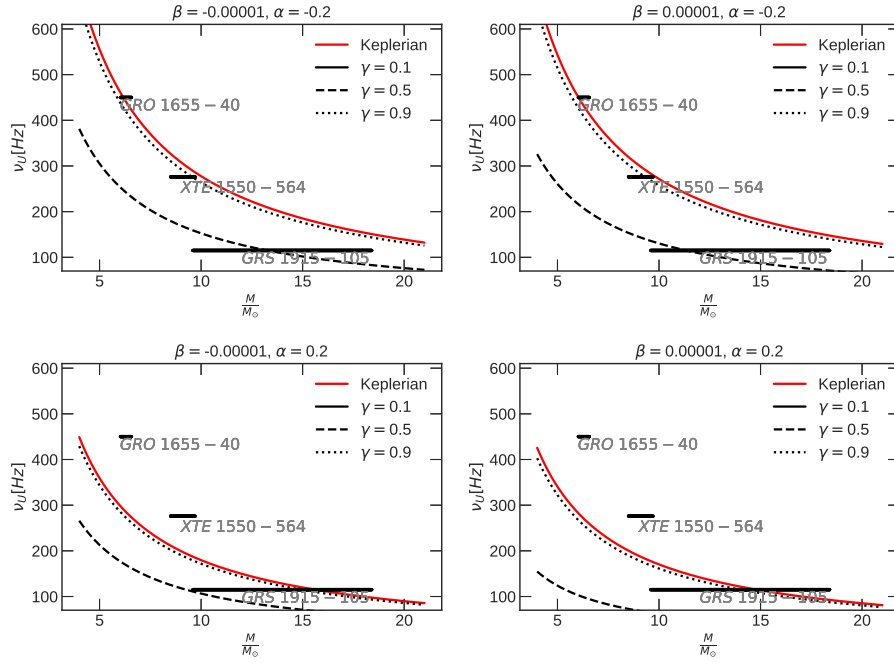


FIG. 10. The upper oscillation frequency ν_U at the resonance radius 3 : 2 is presented for various combinations of the studied parameters for the TD and WD models. For the test-particle is depicted in red. The black lines present the fluid for various angular momentum. If the linestyle does not appear, it means that the chosen ratio 3 : 2 is not possible.

- [9] A. N. Aliev and Valeri P. Frolov. Five-dimensional rotating black hole in a uniform magnetic field: The gyro-magnetic ratio. *Phys. Rev. D*, 69(8):084022, April 2004.
- [10] Gabriel Török, Pavel Bakala, Eva Šrámková, Zdeněk Stuchlík, and Martin Urbanec. On Mass Constraints Implied by the Relativistic Precession Model of Twin-peak Quasi-periodic Oscillations in Circinus X-1. *Astrophys. J.*, 714(1):748–757, May 2010.
- [11] Pavel Bakala, Eva Šrámková, Zdeněk Stuchlík, and Gabriel Török. On magnetic-field-induced non-geodesic corrections to relativistic orbital and epicyclic frequencies. *Classical and Quantum Gravity*, 27(4):045001, February 2010.
- [12] Gabriel Török, Pavel Bakala, Eva Šrámková, Zdeněk Stuchlík, Martin Urbanec, and Kateřina Goluchová. Mass-Angular-momentum Relations Implied by Models of Twin Peak Quasi-periodic Oscillations. *Astrophys. J.*, 760(2):138, December 2012.
- [13] Andres F. Gutierrez-Ruiz, Cesar A. Valenzuela-Toledo, and Leonardo A. Pachon. Innermost Stable Circular Orbits and Epicyclic Frequencies Around a Magnetized Neutron Star. *arXiv e-prints*, page arXiv:1309.6396, September 2013.
- [14] Bushra Majeed, Mubasher Jamil, and Saqib Hussain. Particle Dynamics Around Weakly Magnetized Reissner-Nordström Black Hole. *arXiv e-prints*, page arXiv:1411.4811, November 2014.
- [15] Martin Kološ, Zdeněk Stuchlík, and Arman Tursunov. Quasi-harmonic oscillatory motion of charged particles around a Schwarzschild black hole immersed in a uniform magnetic field. *Classical and Quantum Gravity*, 32(16):165009, August 2015.
- [16] Zdeněk Stuchlík and Martin Kološ. Acceleration of the charged particles due to chaotic scattering in the combined black hole gravitational field and asymptotically uniform magnetic field. *European Physical Journal C*, 76:32, January 2016.
- [17] Mustapha Azreg-Ainou. Vacuum and nonvacuum black holes in a uniform magnetic field. *European Physical Journal C*, 76(7):414, July 2016.
- [18] Bobur Turimov, Bobir Toshmatov, Bobomurat Ahmedov, and Zdeněk Stuchlík. Quasinormal modes of magnetized black hole. *Phys. Rev. D*, 100(8):084038, October 2019.
- [19] Ahmadjon Abdurjabbarov, Javlon Rayimbaev, Farruh Atamurotov, and Bobomurat Ahmedov. Magnetized Particle Motion in γ -Spacetime in a Magnetic Field. *Galaxies*, 8(4):76, October 2020.
- [20] Miao Yi and Xin Wu. Dynamics of charged particles around a magnetically deformed Schwarzschild black hole. *Phys. Scr.*, 95(8):085008, August 2020.
- [21] Robert V. Wagoner, Alexander S. Silbergleit, and Manuel Ortega-Rodríguez. “Stable” Quasi-periodic Oscillations and Black Hole Properties from Diskoseismology. *ApJ*, 559(1):L25–L28, September 2001.
- [22] Shoji Kato. Basic Properties of Thin-Disk Oscillations¹. *PASJ*, 53(1):1–24, February 2001.
- [23] L. Rezzolla, S’i. Yoshida, T. J. Maccarone, and O. Zanotti. A new simple model for high-frequency quasi-periodic oscillations in black hole candidates. *MNRAS*, 344(3):L37–L41, September 2003.
- [24] Robert V. Wagoner. Diskoseismology and QPOs Confront Black Hole Spin. *ApJ*, 752(2):L18, June 2012.
- [25] Z. Stuchlík, A. Kotrlová, and G. Török. Multi-resonance orbital model of high-frequency quasi-periodic oscillations: possible high-precision determination of black hole and neutron star spin. *Astron Astroph*, 552:A10, April 2013.

- [26] G. Török, K. Goluchová, J. Horák, E. Šrámková, M. Urbanec, T. Pecháček, and P. Bakala. Twin peak quasi-periodic oscillations as signature of oscillating cusp torus. *MNRAS*, 457(1):L19–L23, March 2016.
- [27] Marcio G. B. de Avellar, Oliver Porth, Ziri Younsi, and Luciano Rezzolla. KiloHertz QPOs in low-mass X-ray binaries as oscillation modes of tori around neutron stars - I. *MNRAS*, 474(3):3967–3975, March 2018.
- [28] Bhupendra Mishra, Wlodek Kluźniak, and P. Chris Fragile. Relativistic, axisymmetric, viscous, radiation hydrodynamic simulations of geometrically thin discs. II. Disc variability. *MNRAS*, 497(1):1066–1079, September 2020.
- [29] Shoji Kato and Mami Machida. A possible origin of kilohertz quasi-periodic oscillations in low-mass X-ray binaries. *PASJ*, 72(3):38, June 2020.
- [30] A. Kotrlová, E. Šrámková, G. Török, K. Goluchová, J. Horák, O. Straub, D. Lančová, Z. Stuchlík, and M. A. Abramowicz. Models of high-frequency quasi-periodic oscillations and black hole spin estimates in Galactic microquasars. *Astron Astroph*, 643:A31, November 2020.
- [31] Olindo Zanotti, Luciano Rezzolla, and José A. Font. Quasi-periodic accretion and gravitational waves from oscillating ‘toroidal neutron stars’ around a Schwarzschild black hole. *Monthly Notices of the Royal Astronomical Society*, 341(3):832–848, 05 2003.
- [32] Luciano Rezzolla, Shin’ichirou Yoshida, and Olindo Zanotti. Oscillations of vertically integrated relativistic tori – I. Axisymmetric modes in a Schwarzschild space-time. *Monthly Notices of the Royal Astronomical Society*, 344(3):978–992, 09 2003.
- [33] Pedro J. Montero, Luciano Rezzolla, and Shin’ichirou Yoshida. Oscillations of vertically integrated relativistic tori - II. Axisymmetric modes in a Kerr space-time. *MNRAS*, 354(4):1040–1052, November 2004.
- [34] S. Faraji and A. Trova. Dynamics of charged particles and quasi-periodic oscillations in the vicinity of a distorted, deformed compact object embedded in a uniform magnetic field. *MNRAS*, 513(3):3399–3413, July 2022.
- [35] B. P. Abbott, R. Abbott, and et.al. Abbott. Observation of gravitational waves from a binary black hole merger. *Phys. Rev. Lett.*, 116:061102, Feb 2016.
- [36] Fintan D. Ryan. Gravitational waves from the inspiral of a compact object into a massive, axisymmetric body with arbitrary multipole moments. *Phys. Rev. D*, 52(10):5707–5718, 1995.
- [37] M. Abramowicz, M. Jaroszynski, and M. Sikora. Relativistic, accreting disks. *Astron Astroph*, 63:221–224, February 1978.
- [38] Lei Qian, M. A. Abramowicz, P. C. Fragile, J. Horák, M. Machida, and O. Straub. The Polish doughnuts revisited. I. The angular momentum distribution and equipressure surfaces. *Astron Astroph*, 498(2):471–477, May 2009.
- [39] N. I. Shakura and R. A. Sunyaev. Black holes in binary systems. Observational appearance. *Astron Astroph*, 24:337–355, 1973.
- [40] I. D. Novikov and K. S. Thorne. Astrophysics of black holes. In C. Dewitt and B. S. Dewitt, editors, *Black Holes (Les Astres Occlus)*, pages 343–450, 1973.
- [41] F. H. Shu. *The physics of astrophysics. Volume II: Gas dynamics*. 1992.
- [42] W. Kluźniak, M. A. Abramowicz, S. Kato, W. H. Lee, and N. Stergioulas. Nonlinear Resonance in the Accretion Disk of a Millisecond Pulsar. *ApJ*, 603(2):L89–L92, March 2004.
- [43] Both of these terms are collectively referred to as inertial–acoustic waves.
- [44] Hermann Weyl. Zur gravitationstheorie, 1917.
- [45] David M. Zipoy. Topology of some spheroidal metrics, 1966.
- [46] B. H. Voorhees. Static axially symmetric gravitational fields, Nov 1970.
- [47] Hernando Quevedo. Exterior and interior metrics with quadrupole moment, 2011.
- [48] Hernando Quevedo. Mass Quadrupole as a Source of Naked Singularities, Jan 2011.
- [49] F. J. Ernst. Black holes in a magnetic universe. *Journal of Mathematical Physics*, 17(1):54–56, 1976.
- [50] Shokoufe Faraji. Circular geodesics in a new generalization of q-metric. *Universe*, 8(3), 2022.
- [51] S. Kato and J. Fukue. Trapped Radial Oscillations of Gaseous Disks around a Black Hole. *PASJ*, 32:377, January 1980.
- [52] Shokoufe Faraji. Circular geodesics in the generalized q-metric, October 2020.
- [53] G. Török, M. A. Abramowicz, W. Kluźniak, and Z. Stuchlík. The orbital resonance model for twin peak kHz quasi periodic oscillations in microquasars. *Astron Astroph*, 436(1):1–8, June 2005.
- [54] A. Kotrlová, E. Šrámková, G. Török, Z. Stuchlík, and K. Goluchová. Super-spinning compact objects and models of high-frequency quasi-periodic oscillations observed in Galactic microquasars. II. Forced resonances. *Astron Astroph*, 607:A69, November 2017.
- [55] Martin Kološ, Arman Tursunov, and Zdeněk Stuchlík. Possible signature of the magnetic fields related to quasi-periodic oscillations observed in microquasars. *European Physical Journal C*, 77(12):860, December 2017.
- [56] Marek A. Abramowicz, Wlodek Kluźniak, Zdeněk Stuchlík, and Gabriel Török. Twin peak QPOs frequencies in microquasars and Sgr A*. The resonance and other orbital models. In *RAGtime 4/5: Workshops on black holes and neutron stars*, pages 1–23, December 2004.
- [57] G. Török, A. Kotrlová, E. Šrámková, and Z. Stuchlík. Confronting the models of 3:2 quasiperiodic oscillations with the rapid spin of the microquasar GRS 1915+105. *Astron Astroph*, 531:A59, July 2011.
- [58] Luigi Stella and Mario Vietri. Strong Field Gravity and Quasi-Periodic Oscillations from Low-Mass X-Ray Binaries. In Vahe G. Gurzadyan, Robert T. Jantzen, and Remo Ruffini, editors, *The Ninth Marcel Grossmann Meeting*, pages 426–437, December 2002.
- [59] A. Čadež, M. Calvani, and U. Kostić. On the tidal evolution of the orbits of low-mass satellites around black holes. *Astron Astroph*, 487(2):527–532, August 2008.
- [60] U. Kostić, A. Čadež, M. Calvani, and A. Gomboc. Tidal effects on small bodies by massive black holes. *Astron Astroph*, 496(2):307–315, March 2009.
- [61] Shoji Kato. Resonant Excitation of Disk Oscillations by Warps: A Model of kHz QPOs. *PASJ*, 56:905–922, October 2004.